Available online at www.sciencedirect.com
SCIENCE DIRECT®
PERGAMON
International Journal of Heat and Mass Transfer 46 (2003) 1841–1854
International Journal of HEAT and MASS TRANSFER
www.elsevier.com/locate/ijhmt

Saturation boiling of HFE-7100 from a copper surface, simulating a microelectronic chip

Mohamed S. EL-Genk *, Huseyin Bostanci

Department of Chemical and Nuclear Engineering, Institute for Space and Nuclear Power Studies, The University of New Mexico, Farris Engineering Ctr, Room 239, Albuquerque, NM 87131-1341, USA

Received 5 February 2002; received in revised form 28 October 2002

Abstract

Experiments are performed, which investigated the effect of inclination angle, θ, on saturation pool boiling of HFE-7100 dielectric liquid from a smooth, 10×10 mm copper surface, simulating a microelectronic chip. For $\theta \leqslant 90°$ and surface superheats, $\Delta T_{sat} > 20$ K, nucleate boiling heat flux decreases with increased θ, but increases with θ for $\Delta T_{sat} < 20$ K. Similarly, at higher inclinations and $\Delta T_{sat} > 13$ K, nucleate boiling heat flux decreases with increased inclination, but at lower surface superheats the trend is inconclusive. The developed nucleate boiling correlation is within $\pm 10\%$ of the data and the developed correlations for critical heat flux (CHF) and the surface superheat at CHF are within $\pm 3\%$ and $\pm 8\%$ of the data, respectively. Results show that CHF decreases slowly from 24.45 W/cm^2 at 0° to 21 W/cm^2 at 90°, then decreases fast with increased θ to 4.30 W/cm^2 at 180°. The surface superheat at CHF also decreases with θ, from 31.7 K at 0° to 19.9 K at 180°. Still photographs are recorded of pool boiling at different heat fluxes and $\theta = 0°$, 30°, 60°, 90, 120°, 150° and 180°. The measured average departure bubble diameter from the photographs taken at the lowest nucleate boiling heat flux of ~ 0.5 W/cm^2 and $\theta = 0°$ is 0.55 ± 0.07 mm and the calculated departure frequency is ~ 100 Hz.

Keywords: Dielectric liquids; HFE-7100; Nucleate boiling; Critical heat flux; Departure bubble diameter and departure frequency; Immersion cooling of electronics, and high performance chips

1. Introduction

During the last decade, the phenomenal increases in clock speed and transistors density in microelectronic chips, while decreasing the size and surface area, have significantly increased the heat dissipation and the dissipation heat flux from the CPU. Not only the cooling requirements for the chips have to be met, but also their junction temperature need to be maintained within an acceptable range, typically 85–100 °C, or even lower, depending on the type of the chip and the application. Excessive temperatures induce stresses and could melt the solder joints as well as cause laminate out-gassing, oxidation, and materials migration, shortening the useful lifetime and increasing the failure frequency of the chips [1]. The frequency of "thermally-induced" failures increases exponentially with the chip temperature above recommended values, typically 70–85 °C; a 10–15 °C increase above such temperatures could halve the operation lifetime of the chip [2]. Therefore, adequate cooling is a key to maintaining the microelectronic devices working properly and, hence, achieving high performance reliability.

The cooling of computer and microprocessor chips is further constrained by the temperature difference between the chip and the ultimate heat sink (e.g., ambient air), which depends on the cooling method used. For dissipation heat fluxes $\leqslant 0.3$ W/cm^2, forced convection air cooling is adequate, and for fluxes up to 10–15 W/cm^2

* Corresponding author. Tel.: +1-505-277-5442; fax: +1-505-277-2814.
E-mail address: mgenk@unm.edu (M.S. EL-Genk).

0017-9310/03/$ - see front matter
doi:10.1016/S0017-9310(02)00489-1

advanced forced convection liquid cooling and cooling with air or liquid jets could be adequate. For higher dissipation heat fluxes, cooling with nucleate boiling is promising, as it removes dissipated heat within a wide range of fluxes and at relatively small surface temperature superheats. For cooling with nucleate pool boiling, however, most candidate liquids are electrically conductor (non-dielectric), needing to be electrically insulated from the chip, which increases the heat transfer resistance and raises the junctions' temperature. In addition, these liquids could be chemically corrosive to be maintained in confined ducts. An alternative is immersion cooling by nucleate boiling of dielectric liquids, which offer a wide range of saturation temperatures (40–85 °C) for diverse cooling applications. In immersion cooling, the boiling liquid contacts both the chips and the circuit board on which they are mounted. Recent studies have indicated that the dissipated heat from an immersed chip with a smooth copper surface can be removed by nucleate boiling of FC-72 dielectric liquid at surface fluxes $\geqslant 15$ W/cm^2 [3–6]. Currently, the dissipation heat flux from high performance computer may exceed 50 W/cm^2, and could reach 100 W/cm^2 in a few years. Nucleate boiling of dielectric liquids could meet the current and projected near term cooling requirements for high performance computer chips.

The cooling with nucleate boiling of dielectric liquids offers several advantages, namely: (a) low saturation temperatures (<100 °C at 0.1 MPa, e.g., see Table 1) and small temperature variation across the surface, hence eliminating hot spots; (b) adequate cooling in "tight" spaces; (c) excellent corrosion properties and chemical compatibility with the chip surface; and (d) safe handling and low boiling temperatures, making it possible to use plastic containers. In addition, dielectric liquids are environmentally friendly with zero Ozone depletion potential and low global warming potential (Table 1). However, owing to their high wetting property (or very low surface tension), dielectric liquids fill surface crevices, delaying incipient nucleation to a relatively high surface superheat, which needs to be determined and accounted for in electronics cooling applications. In addition, dielectric liquids need to be used in tightly sealed containers to prevent leakage. The Fluorinert C_6F_{14}, or FC-72, dielectric liquid, and to some extent FC-86 and FC-87, is being used in electronics cooling and its cooing potential has been investigated in a number of pool boiling experiments, e.g. [3–7]. Little work, however, has been reported, on Novec liquids, recently introduced by 3M Company, such as HFE-7100 ($C_4F_9OCH_3$) and FC-7200 ($C_4F_9OC_2H_5$). In addition to having much lower global warming potential than Fluorinert liquids, Novec liquids have larger latent heats of vaporization (Table 1) and, hence, the potential to achieve higher nucleate boiling and critical heat flux (CHF). Table 1 compares the physical properties of

Table 1
A comparison of physical properties of the HFE-7100 and FC-72 dielectric liquids

Saturation physical properties	HFE-7100 (0.1 MPa) ($C_4F_9OCH_3$)	HFE-7100 (0.085 MPa[a])	FC-72 (0.1 MPa) (C_6F_{14})
Boiling point (°C)	61	54	56
Freeze point (°C)	−135	−135	−90
Ave. molecular weight (g/mole)	250	250	338
Liquid density (kg/m^3)	1370.2	1388.7	1602.2
Vapor density (kg/m^3)	9.87	8.00	13.21
Liquid viscosity (kg/m s)	3.70×10^{-4}	3.89×10^{-4}	4.33×10^{-4}
Liquid specific heat (J/kg K)	1255	1241	1101
Latent heat of vaporization (kJ/kg)	111.6	111.6	88
Liquid thermal conductivity (W/m K)	0.062	0.063	0.054
Liquid surface tension (N/m)	1.019×10^{-2}	1.084×10^{-2}	7.93×10^{-3}
Environmental properties	HFE-7100	FC-72	
Ozone depletion potential[b]—ODP	0.00	0.00	
Global warming potential[c]—GWP	320	7400	
Atmospheric lifetime-ALT (yrs)	4.1	3200	
Electrical properties @25 °C	HFE-7100	FC-72	
Dielectric strength (kV 0.1″ gap)	28	38	
Dielectric constant	7.39 (100 Hz–10 MHz)	1.75 (1 KHz)	
Volume resistivity (Ω cm)	3.3×10^9	1.0×10^{15}	

[a] Atmospheric pressure in Albuquerque, NM.
[b] CFC-11 = 1.0.
[c] GWP-100 year integration time horizon (ITH).

HFE-7100 at 0.1 and at 0.085 MPa (the atmospheric pressure in Albuquerque, NM), and of FC-72 at 0.1 MPa.

Chang and You [4] have investigated the effect of θ on saturation boiling of FC-72 from 10×10 mm, smooth copper surface. They reported that at high surface superheats, the nucleate boiling heat flux increased as θ increased from 0° (upward-facing) to 90° (vertical). However, for $\theta > 90°$, they reported a noticeable decrease in the nucleate boiling heat flux as θ was increased. For a 20×20 mm surface, Chang and You [5] have reported an increase in the nucleate boiling heat flux with increased θ from 0° to 45°, but a decrease with $\theta > 45°$. Recently, Rainey [6] has reported for saturation boiling of FC-72 from a 50×50 mm smooth copper surface that at low surface superheats nucleate boiling heat flux increased slightly with increased θ from 0° to 45°, then decreased with increased θ beyond 45°.

The HFE-7100 dielectric liquid, which is the subject of this investigation, shares many of the excellent thermal and physical properties of FC-72, but offers a higher cooling potential by nucleate boiling [8]. Additional work is needed to quantify this cooling potential at saturation condition and develop useful correlations for future design use and implementation. Additional work is also needed to better quantify the effect of surface inclination on nucleate boiling, CHF, the overshoot in surface temperature at incipient boiling, and the surface superheat at CHF. The latter two are important to the determination of the maximum junctions temperature of the chips cooled by nucleate boiling of HFE-7100 dielectric liquid. The results would help quantifying the effect of orientation on cooling the CPU by nucleate boiling of HFE-7100 in various packing arrangements.

A series of saturation pool boiling experiments of HFE-7100 liquid from 1 cm^2, smooth copper surface, simulating a high performance computer chip, is performed to investigate the effect of surface inclination on both nucleate boiling and CHF. In the experiments, $\theta = 0°$, 30°, 60°, 90°, 120°, 150°, 170°, and 180°, and the values of the surface temperature superheat at CHF and surface temperature overshoot at incipient boiling are measured. The data for the nucleate boiling heat flux, q''_{NB}, CHF, and the surface superheat at CHF are correlated as functions of θ. In addition, still photographs of the boiling surface are taken using high quality digital camera at different nucleate boiling heat fluxes, surface superheats, ΔT_{sat}, and $\theta = 0°$, 30°, 90°, 120°, 150° and 180°. The photographs taken when $\theta = 0°$ at the lowest nucleate boiling heat flux (~0.5 W/cm^2), where the surface is covered with a fewer bubbles, are used to determine the average departure bubble diameter, after the images are electronically enhanced and magnified. Based on the measured average departure diameter, the bubble departure frequency is calculated.

2. Experimental setup and conduct

The pool boiling experimental facility used in the present investigation (Fig. 1), is comprised of the following major components: (a) a heated water bath in an acrylic tank ($318 \times 318 \times 514$ mm), (b) an acrylic test vessel (Fig. 2a), measuring $149 \times 130 \times 343$ mm, (c) the test section mounted onto a rotation assembly (Fig. 2b), (d) a control unit of the water bath temperature, (e) a DC power supply for the Nichrome wire heating element in test section, (f) a computer controlled data acquisition unit, (g) an electrical power control circuit with a shunt resistor for measuring the electric current to the Nichrome heating element, (d) a control unit (Variac) of the electric power to the 1500 W, AC heater of the water bath, and (h) a cooling water loop for the submerged and reflux condensers in test vessel (Figs. 1 and 2c). The electrical heater of the water bath is immersed at the bottom of the tank to maximize mixing by natural convection and maintain a uniform bath temperature at or slightly above saturation temperature of the HFE-7100 liquid (~54 °C, see Table 1). The temperature of the water bath is measured using a K-type thermocouple connected to the control unit of the immersion heater to maintain the bath temperature to with ±0.5 K of the desired value. To speed out-gassing of the HEF-7100 liquid pool and ensure uniform pool temperature prior to conducting the experiments, a magnetic stirrer is placed at the bottom of the test vessel and spun using an external power unit (Fig. 2a). Owning to the high air solubility, it took about 2 h to fully outgas the HFE-7100 pool.

The HFE-7100 test vessel is tightly sealed to prevent leakage and loss of the test liquid in the experiments. The cover plate is fitted with a rubber O-ring and fastened to the vessel wall using eight, stainless steel bolts and nuts (Fig. 2c). The water-cooled reflux condenser on the inside of the cover plate of the test vessel effectively condenses the vapor produced in the experiments, hence maintaining a constant liquid level in the pool (Fig. 2c). A small, water-cooled copper coil is immersed into the HFE-7100 pool for fine adjustment of its temperature in subcooled boiling experiments, which will be presented in a separate report. The HFE-7100 temperature is taken as the average reading of the two, K-type thermocouples immersed in the pool, on opposite sides of the test section (Fig. 2a).

The acrylic used to manufacture the tank for the water bath and the test vessel is lightweight, has high impact resistance and excellent chemical compatibility and machinability, and is more than 90% transparent and optically clear. The latter is important for taking high quality, still photographs of the boiling surface from outside the water bath tank. The submerged test section in the HFE-7100 pool is mounted to a rotation assembly (Fig. 2b). All parts of the rotation assembly,

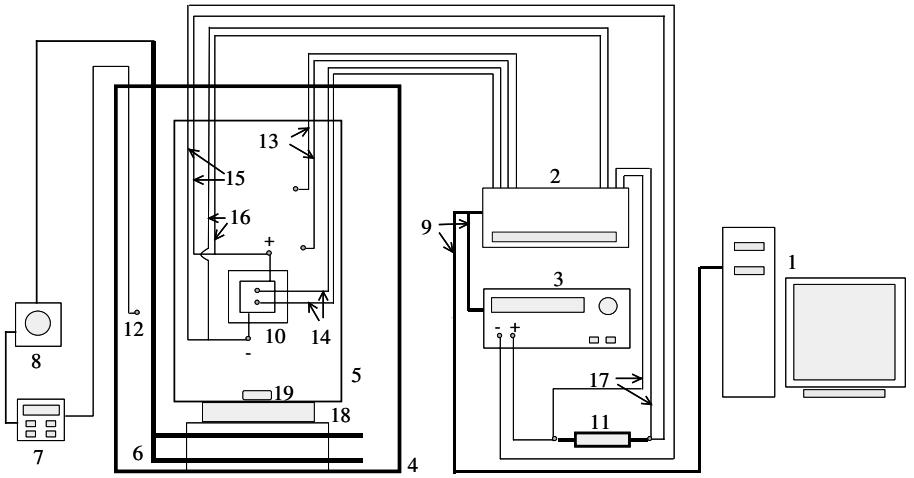

1: PC & GPIB board, 2: Data acquisition unit, 3: Programmable DC power supply, 4: Water bath tank, 5: Test vessel, 6: Immersion heater, 7: Temperature controller, 8: VAC variac, 9: IEEE -488.2 cables, 10: Test section assembly, 11: Shunt resistor, 12: Thermocouple measuring the temperature of water bath, 13: Two thermocouples for measuring the temperature of the test liquid, 14: Two thermocouples for measuring the temperature of boiling surface, 15: Electric power cables to the heating element, 16: Cables for voltage measurement across the heating element, 17: C ables for voltage measurement across the shunt resistor (11), 18: Magnetic stirrer power unit, 19: Magnetic stirrer bar.

Fig. 1. The present facility used to conduct the pool boiling experiments for HFE-7100 liquid.

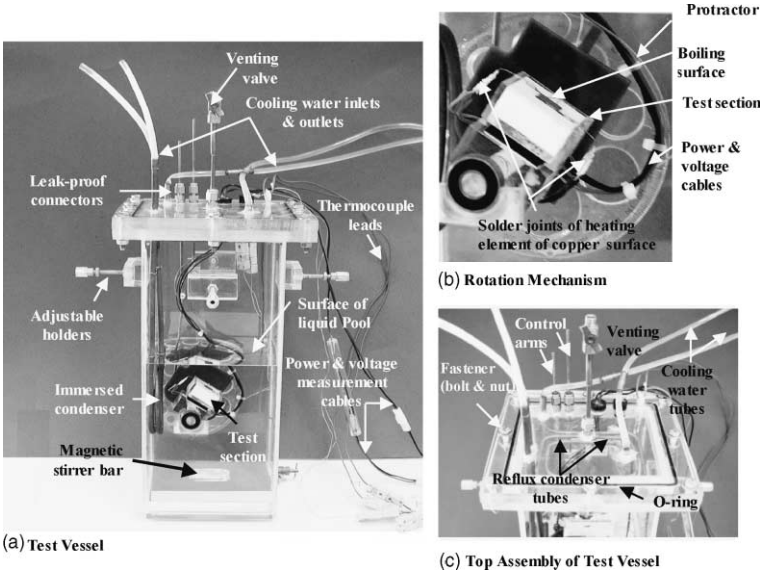

Fig. 2. The test vessel for pool boiling experiments and rotation mechanism of the test section.

except the two-roll bearings mounted on the inside of the test vessel wall, are acrylic. The rotation assembly changes the inclination angle of the mounted test section (Fig. 2b) from 0° inclination to 180° in small increments, without obstructing the boiling surface. This is accomplished using a special slider-crank mechanism composed of five connected arms, which are manipulated through the top plate of the test vessel (Fig. 2c). The acrylic protractor, mounted onto the outside of one of the sidewalls of the test vessel (Fig. 2b), is used to measure the inclination angle of test section in the experiments.

2.1. Test section

The test section consists of a Teflon block, $30 \times 30 \times 12.7$ mm (Fig. 3), that has a square cavity, $10.1 \times 10.1 \times 1.0$ mm, in the center of the top surface for installing the heating element and the overlying copper block, $10 \times 10 \times 1.63$ mm (Fig. 3). The heating element made of a wound, 0.125 mm diameter Nichrome wire, has a total resistance of 14 Ω. The thin layer of high thermally conductivity and high electrical resistivity epoxy that covers the wound wire is cured under an infrared lamp at ~100 °C for 2 h. After the assembled test section is fully cured, two copper leads, ~0.5 mm in diameter, are soldered to the ends of the Nichrome wire to reduce electrical and heat losses outside the heating element (Fig. 3b). In addition, two, K-type thermocouples are inserted in two small horizontal holes drilled on one side in the copper block, ~0.8 from the top surface, half way into the block. The measuring tips of the Teflon insulated thermocouples are securely attached to the copper block at the bottom of the 0.5 diameter holes using silver solder. The average reading of these two thermocouples is taken as the copper surface temperature for constructing the pool boiling curves in the experiments.

The test section encased in a Lexan frame with a closed bottom (Fig. 3a and b) is mounted onto the acrylic block in the rotation assembly (Fig. 2b). After the test section is mounted inside the Lexan frame, the shallow cavity at the top of the Teflon block is filled with translucent two part epoxy adhesive, to slightly (<0.1 mm) below the exposed surface of the copper block, preventing any tiny grooves from forming at the edges of the copper surface. Such grooves, if present, would stimulate bubble nucleation before the copper surface becoming hot enough to initiate boiling, skewing the pool boiling curves. Thus, extreme care is taken in applying the translucent epoxy adhesive and ensuring good wetting with the sides of the copper block and the inside surface of the Lexan frame (Fig. 3b). Prior to conducting the experiments, the copper surface is prepared using consistent methodology. It is sanded with emery paper #400 in even strokes to remove scratches and dents then polished with a metal polishing liquid and cleansed with water and alcohol. Finally, the surface is prepared using fine emery paper (#1500) by applying 12 consecutive strokes (five times from left to right, five times from right to left, two times from top to bottom, and two times from bottom to top).

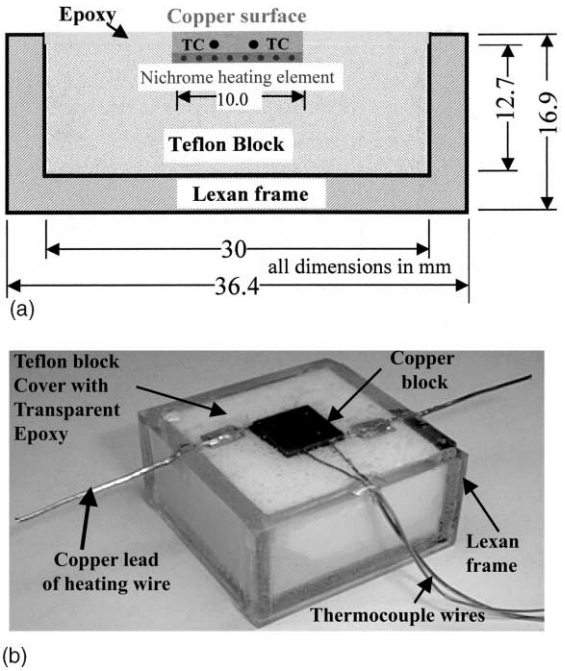

Fig. 3. Cutaway view and photograph of the assembled test section. (a) Cross sectional view and (b) assembled test section.

The electric power to the Nichrome heating wire in the test section is supplied by a DC power supply (Fig. 1), which is controlled and operated by a PC. A shunt resistor (~99.462 mΩ) in the control circuit is used to determine the electrical current from the measured voltage drop across it, while the voltage across the Nichrome wire leads is measured directly (Figs. 1 and 2a). The dissipation heat flux from the copper surface is calculated from the measured current and the voltage across the wire of the heating element.

2.2. Thermal analysis of test section

To size the dimensions of the Teflon block in the test section prior to fabrication, a 3-D, steady state thermal analysis (Fig. 3a) is performed using "Algor", finite elements thermal analysis commercial software, to ensure minimal heat losses from the heating wire through the bottom and the side surfaces of the assembled test section. This analysis is performed at different surface heat fluxes, assuming a uniform nucleate boiling heat transfer coefficient at the copper surface and constant liquid pool temperature of 56 °C. The results for a surface heat flux of 25 W/cm^2 (Fig. 4), show that heat losses are negligible and the temperature of the copper surface is uniform and <0.2 K below that midway in the copper block (Fig. 3a). This confirms that the surface temperature in the experiments could be taken as the average reading of the two thermocouples placed in the copper block (Fig. 3a).

2.3. Experiments conduct

In the experiments, the test section is immersed in the HFE-7100 liquid pool such that the copper surface in the upward-facing position (0°) is at least 10 cm below

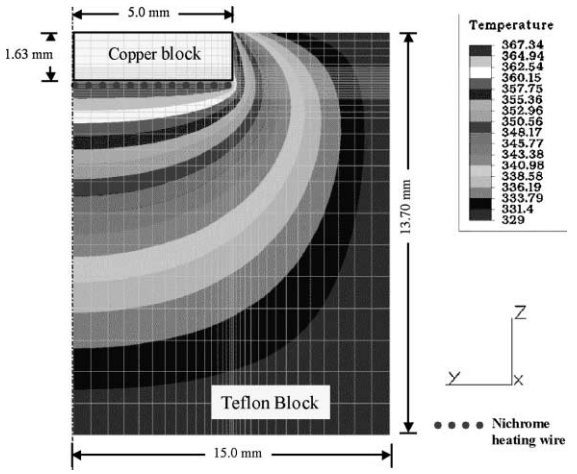

Fig. 4. The calculated temperature field in the assembled test section at surface heat flux of 25 W/cm^2 and pool temperature of 56 °C.

the free surface of the pool (Fig. 2a). Because of the high elevation in Albuquerque, NM (~1500 m above sea level), the saturation temperature of HFE-7100 in the experiments is only 54 °C. The experiments begin by turning off the magnetic stirrer at the bottom of the test vessel and incrementally increasing the electrical power input to the heating element, via increasing the applied voltage to the heating element in increments of $\leqslant 0.3$ V. Following each voltage increase, the surface heat flux and temperature are recorded after reaching steady state. Although steady state is reached ~60 s following an incremental increase in the electric power to the heating element, data are stored after 80 s to ensure steady state condition. To avoid burning the heating wire at CHF, when the difference in the measured steady state surface temperatures, following two successive increases in the electrical power to the heating element, exceeds 10 °C, it is taken as an indication for reaching CHF, and the experiment is terminated. The LabView program developed to conduct the test procedures is capable of terminating the experiments within 40 ms upon sensing CHF, hence protecting the heating element in the test section. The estimated experimental uncertainty in the temperature measurements is ± 0.7 K, $\pm 3.7\%$ in surface heat flux, and $\pm 0.5°$ in the inclination angle θ.

3. Results and discussion

Fig. 5a presents two boiling curves measured at 90°; one is obtained while incrementally increasing the heat flux and the other is obtained while incrementally decreasing the heat flux. Except for the surface temperature overshoot at incipient boiling, the two pool boiling curves are almost identical. Similar results are obtained at other inclinations (Fig. 6), indicating a little or no effect of the method of changing the heat flux in the experiments on the measured pool boiling curves, which is consistent with earlier results by Rini et al. [9] for FC liquids. Other investigators, however, have reported large hysteresis between the saturation pool boiling curves of FC-72 obtained by increasing and by decreasing the heat flux [4,5]. Fig. 5b presents two saturation-boiling curves obtained in two separate tests at the same conditions and 120°, indicating excellent reproducibility of the data.

Fig. 5a and b show that the nucleate boiling curves can be divided into three distinct regions of low (I), intermediate (II) and high (III) surface superheat, in which the heat flux increases linearly, but at a different rate,

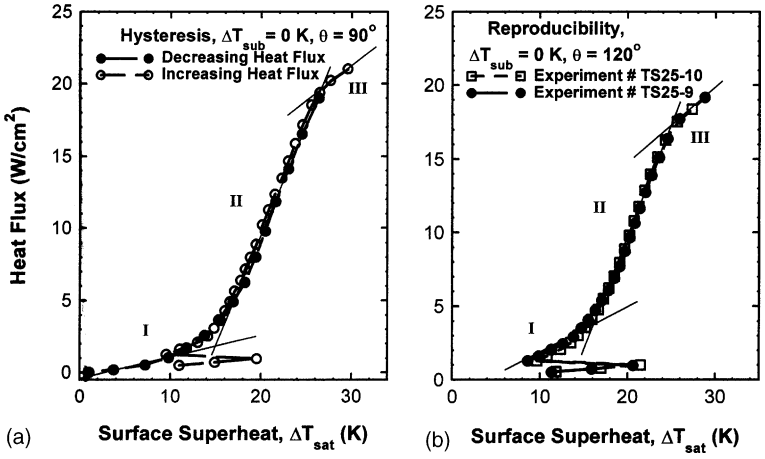

Fig. 5. The obtained nucleate boiling curves for HFE-7100 at 90° and 120°.

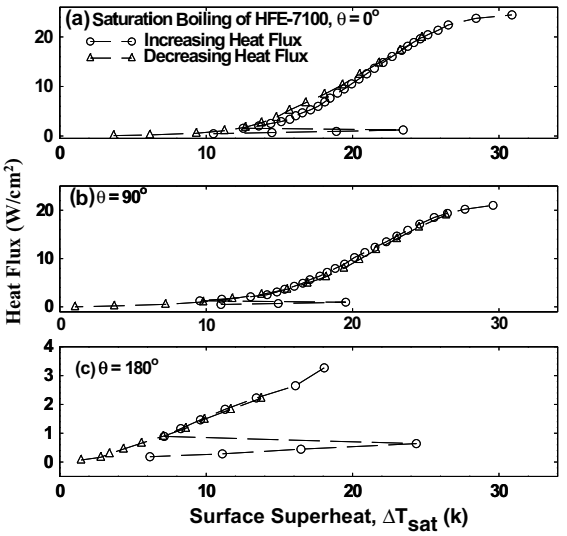

Fig. 6. The nucleate boiling curves for HFE-7100 at 0°, 90° and 180° obtained by increasing and decreasing heat flux in experiments.

with surface superheat. This characteristic is consistent for all inclination angles, except for $\theta > 170°$, only the lower and intermediate superheat regions exist (Figs. 9 and 10). In the low surface superheat region I, the slope of the boiling curve is lowest due to the fewer active nucleation sites on the copper surface. As the number of active nucleation sites increase with increasing surface superheat, the slope of the boiling curves in this region increases. In the intermediate nucleate boiling region II, the number of nucleation sites is highest, resulting in the steepest slope of the boiling curve, where a small increase in the surface superheat results in a large increase in the nucleate boiling heat flux. Near the end of region II, the accumulation and coalescence of departing vapor bubbles near the surface begins to hinder the heat transfer rate, causing the slope of the boiling curve to decrease with increasing the surface superheat until reaching CHF. The still photographs presented later in this paper support the experimental data in Figs. 5–10. In these Figures, the upper most data points in the boiling curves indicate CHF.

Figs. 5 and 6 show that at incipient boiling, the surface superheat varies from 20 to 22 K, versus only 8–10 K in nucleate boiling at almost the same heat flux. The data do not show a clear dependence of the surface superheat at incipient boiling, averaging $\sim 22 \pm 4$ K, on θ (Fig. 7a). This surface superheat corresponds to an average temperature overshoot of 11.6 ± 4 K (Fig. 7b) and an average surface temperature of 349 ± 4 K (or 76 ± 4 °C). Such surface temperature is well below the 85–100 °C temperature limit recommended for most computer chips. Previously reported surface superheats at incipient boiling of FC-72 from a 10×10 mm and a 40×40 mm copper surface [4,5] varied from 25 to 40 K and from 20 to 35 K, respectively, which are much higher than in the present experiments. Rainey [6], however, has reported surface superheats at incipient boiling of only 16–17 K in saturation pool boiling experiments of FC-72 from a 50×50 mm copper surface.

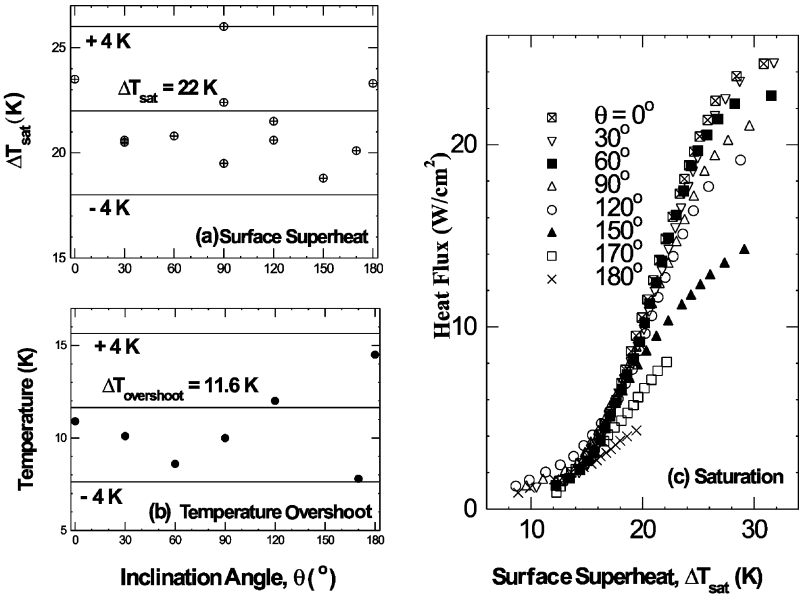

Fig. 7. The measured surface temperature at incipient boiling and saturation boiling curves.

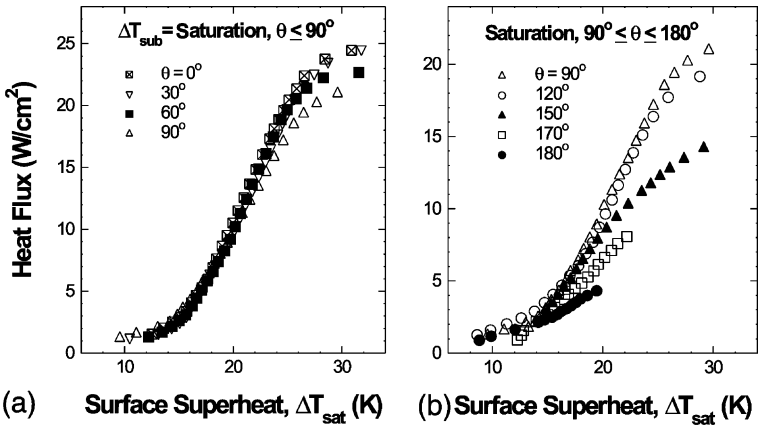

Fig. 8. Saturation pool boiling curves for HFE-7100 liquid at the different inclination angles.

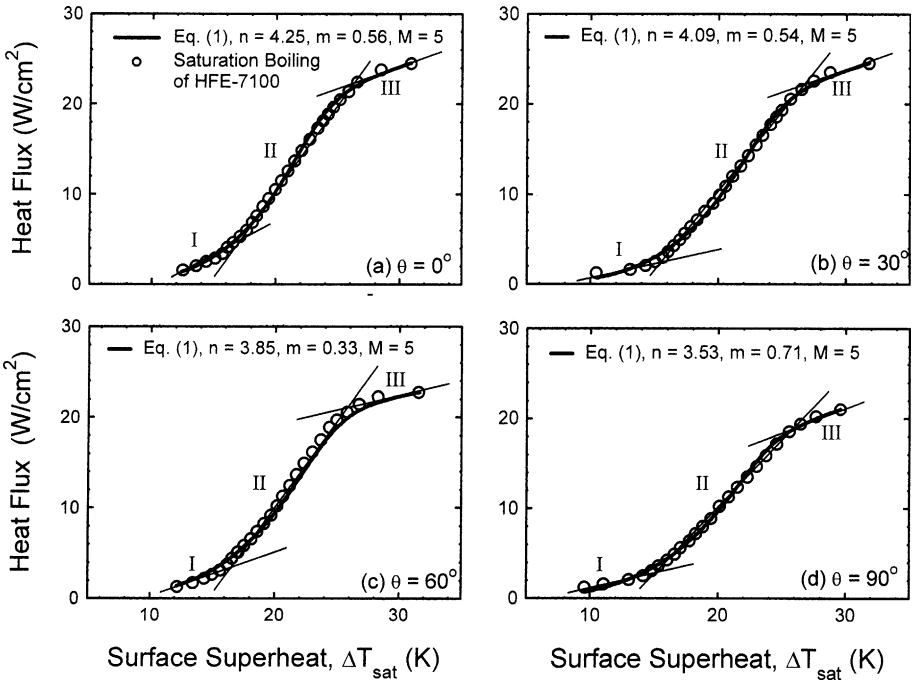

Fig. 9. Nucleate boiling curves and correlation for HFE-7100 at 0°, 30°, 60° and 90° inclinations.

Fig. 7c presents the obtained saturation nucleate boiling curves at eight inclination angles, while Figs. 8a and b present the pool boiling curves for $0° \leqslant \theta \leqslant 90°$ and $90° \leqslant \theta \leqslant 180°$, respectively. As shown in Fig. 8a, at higher surface superheats (>20 K), the nucleate boiling heat flux is highest at 0° and decreases as θ increases to 90° (Fig. 8a), due to the increased accumulation of the vapor bubbles near the surface, in agreement with earlier data for non-dielectric liquids [10,11] and FC-72 [4]. Conversely, at lower superheats, the nucleate boiling heat flux increases with decreasing θ, due to increased mixing in the boundary layer by the departing vapor bubbles from the surface, also consistent with earlier results for non-dielectric liquids [8,9]. The residence time of the sliding bubbles in the boundary layer, before reaching the upper edge of the surface, increases as θ increases, increasing mixing near the surface and, hence, the nucleate boiling heat flux. At higher inclinations, $90° \leqslant \theta \leqslant 180°$, and high surface superheats (>13 K), the nucleate boiling heat fluxes are highest at 90° and de-

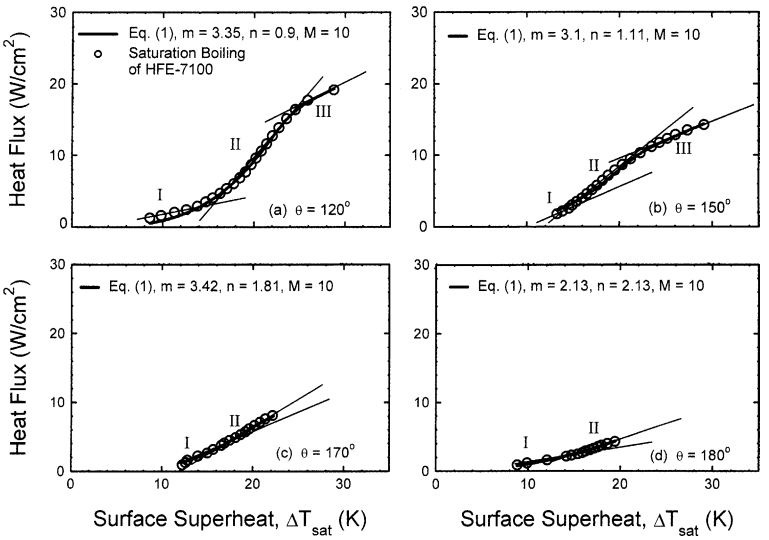

Fig. 10. The obtained nucleate boiling curves for HFE-7100 and correlation at inclinations of 120°, 150°, 170° and 180°.

crease as θ increases to 180° (Figs. 7 and 8b), again due to the accumulation of the vapor bubbles near the surface, in agreement with earlier data for FC-72 [4–6]. At lower surface superheats, however, the dependence of the nucleate boiling heat flux on θ is inconclusive (Fig. 8b).

Figs. 9 and 10 once again show that for $\theta < 170°$, there are three nucleate boiling regions. The low surface superheat region I, starting at ΔT_{sat} as low as 8.5 K (Fig. 10a), in it the nucleate heat flux increases with ΔT_{sat} relatively slow, but at an increasing rate. In the intermediate surface superheat region II ($\Delta T_{sat} \gtrsim 16$ K), the nucleate boiling heat flux increases fastest, at an almost constant rate with increasing ΔT_{sat}. In the high surface superheat region III ($\Delta T_{sat} \gtrsim 26$ K), the nucleate boiling heat flux increases at a declining rate with increasing ΔT_{sat} to CHF. The range of the nucleate boiling heat flux for each region decreases as θ increases. For $\theta = 170°$ and 180°, however, region III disappears and the ranges of the other two nucleate boiling heat flux regions are much smaller than at higher inclinations (Fig. 10c and d).

3.1. Nucleate boiling heat flux correlation

The present saturation nucleate boiling heat flux, q''_{NB}, curves in Figs. 9 and 10 are correlated individually in each of the nucleate boiling regions using linear least square fits. The obtained relations are then combined for each θ using and a power law, yielding the following general relation:

$$q''_{NB} = \left[\left(a\Delta T_{sat}^{n} \right)^{-M} + \left(b\Delta T_{sat}^{m} \right)^{-M} \right]^{(1/M)}. \quad (1)$$

The obtained coefficients and exponents in this correlation as functions of θ are listed in Table 2.

The first term on the right hand side of Eq. (1) is obtained from correlating the nucleate boiling data in the low and intermediate surface superheat regions I and II, while the second term is obtained from correlating the nucleate boiling data in the high surface superheat region III (Figs. 9 and 10). Eq. (1) for all inclinations is in good agreement with the present saturation nucleate boiling data of HFE-7100 to within ±10% (Fig. 11).

Table 2
Coefficients and exponents in nucleate boiling correlation (Eq. (1))

	θ (°)							
	0	30	60	90	120	150	170	180
$a \times 10^4$	0.31	0.46	0.93	0.25	4.40	7.53	2.49	78.4
b	3.60	3.80	7.30	1.90	0.94	0.34	0.0295	0.0
n	4.25	4.09	3.85	3.53	3.35	3.10	3.42	2.13
m	0.56	0.54	0.33	0.71	0.90	1.11	1.81	2.13
M	5	5	5	8	10	10	10	10

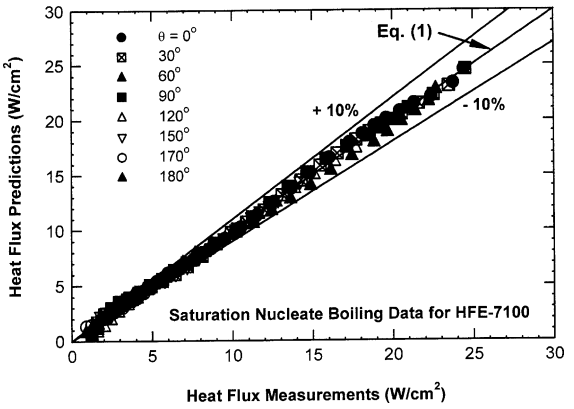

Fig. 11. A comparison of nucleate boiling heat flux measurements with predictions (Eq. (1)).

3.2. Critical heat flux data and correlation

Fig. 12a shows that CHF decreases slowly with increasing inclination for $\theta < 90°$, but much faster at higher θ, consistent with earlier data for FC-72 [4] and for non-dielectric liquids [10,11]. CHF decreases from $\sim$24.5 W/cm^2 at 0° to only $\sim$4.3 W/cm^2 at 180° (Figs. 7c,8,9a and c). The present CHF data are correlated using the form suggested by Kutatelatze [12], and which has been used successfully to correlate the saturation CHF data for water, liquid helium and liquid nitrogen [11] as functions of θ. The developed correlation for the present saturation CHF data of the HFE-7100 liquid is:

$$\mathrm{CHF}_{\mathrm{sat}} = C_{\mathrm{CHF,sat}}(\theta)\rho_{\mathrm{v}}^{0.5} h_{\mathrm{fg}}[\sigma g(\rho_{\ell} - \rho_{\mathrm{v}})]^{0.25}, \quad (2)$$

where

$$C_{\mathrm{CHF,sat}}(\theta) = \left[\left(0.229 - 4.27 \times 10^{-4}\theta\right)^{-6} + \left(0.577 - 2.98 \times 10^{-3}\theta\right)^{-6}\right]^{(-1/6)}. \quad (3)$$

In Eq. (2), ρ_{v}, ρ_{ℓ}, h_{fg}, and σ are the liquid density, vapor density, latent heat of vaporization, and surface tension of HFE-7100 at saturation temperature (Table 1), respectively, and g is the acceleration of gravity. As shown in Fig. 12a, Eq. (3) agrees with the present CHF data to within ±3%. The lowest and the highest values of the coefficient $C_{\mathrm{CHF,sat}}$ are 0.041 and 0.229 at 180° and 0°, respectively. These values are higher than those reported for non-dielectric liquids at the same inclinations [10,11]. El-Genk and Guo [11] have shown that $C_{\mathrm{CHF,sat}}$ varies not only with θ, but also with the properties of the boiling liquid. For example, at 0° they reported a value of 0.145 for saturation boiling of water, and 0.1485 and 0.1385 for saturation boiling of liquid helium and liquid nitrogen, respectively.

The present CHF values for HFE-7100 are normalized to that at 0° and plotted in Fig. 12b, together with the normalized values of the reported CHF by Chang and You [4,5] and Rainey [6] for FC-72. Chang and You have reported CHF values of 15.6 W/cm^2 and 2.1 W/cm^2 for FC-72 at 0° and 180°, respectively, which are $\sim$63% and 48% of the present values for HFE-7100 at the same inclinations, respectively. Despite the large difference in

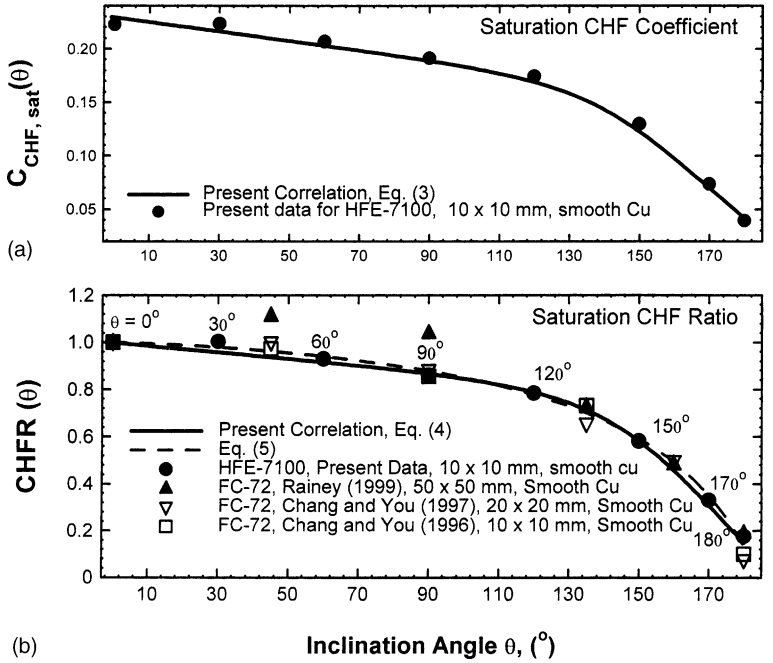

Fig. 12. The data and correlations showing the effect of θ on CHF and CHFR for both HF-7100 and FC-72 dielectric liquids.

the actual CHF values, the normalized values (or CHFR) for HFE-7100 and FC-72 are very close and decrease with increased inclination to their lowest values at 180° (Fig. 12b). For these two liquids, CHFR decreases linearly, at a small slope, with increased inclination for $\theta < 90°$, but much faster for $\theta > 90°$. The CHFR data for both HFE-7100 and FC-72 [4–6] are correlated as a function of θ (Fig. 12b) as:

$$\mathrm{CHFR}(\theta) = \left[(1 - 0.00127\theta)^{-4} + (3.03 - 0.016\theta)^{-4}\right]^{(-0.25)}. \quad (4)$$

The same CHFR data are also correlated using the general form proposed by Chang and You [4] for correlating the CHF data for FC-72, (Fig. 12b), which yields:

$$\mathrm{CHFR}(\theta) = 1.0 - (0.00123\theta\tan(0.414\theta) - 0.080\sin(0.318\theta)). \quad (5)$$

Eqs. (4) and (5) agree with the data in Fig. 12b to within ±8%, except those for the 170° and 180° inclinations are within ±20–40% of the data, because of the sensitivity of the CHF measurements to the uncertainty in adjucting θ close to the downward-facing position (180°). Fig. 12b demonstates that CHFR values for HFE-7100 and FC-72 are not only very close, but also independent of the size of the copper surface used in the experiments.

Fig. 13a and b show that both the surface superheat and the surface temperature at CHF decrease as θ increases, with their highest values of 31.7 and 85.7 °C, respectively, occurring at 0°. At 180°, however, the surface superheat and surface temperature at CHF of 19.9 K and 73.9 °C, respectively, are the lowest. The decreases in the surface superheat and surface temperature at CHF with increasing inclination are small for $\theta \geqslant 60°$, but quite step at higher θ. The values of the surface superaheat at CHF for HFE-7100 are correlated as a function of θ as (Fig. 13a):

$$\Delta T_{\mathrm{sat}}(K) = 31.7 + 2.6 \times 10^{-3}\theta - 2.1 \times 10^{-6}\theta^3. \quad (6)$$

The corresponding surface temperature is given as, $T_{\mathrm{sur}} = T_{\mathrm{sat}}(54\ °\mathrm{C}) + \Delta T_{\mathrm{sat}}$ (Fig. 13b). The results indicate that the measured surface temperatures at CHF in the present experiments ($\leqslant 85.7$ °C) are below the limit for the junction temperature for most high performance computer chips (~100 °C). Eq. (6) is plotted versus Eq. (2) in Fig. 14. The predictions based on these two equations are indicated in the figure by the solid line, while the dashed line is a spline fit of the present data. Fig. 14 shows that the CHF values at 0° and 30° are very close, while the surface superheat for the latter is slightly higher. For high inclinations, however, both CHF and the corresponding surface superheat decrease monotonically with increasing θ, reaching their lowest values at 180° (downward-facing).

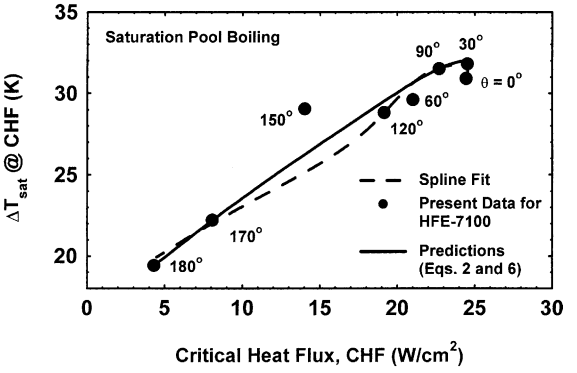

Fig. 14. Saturation CHF versus surface superheat at CHF.

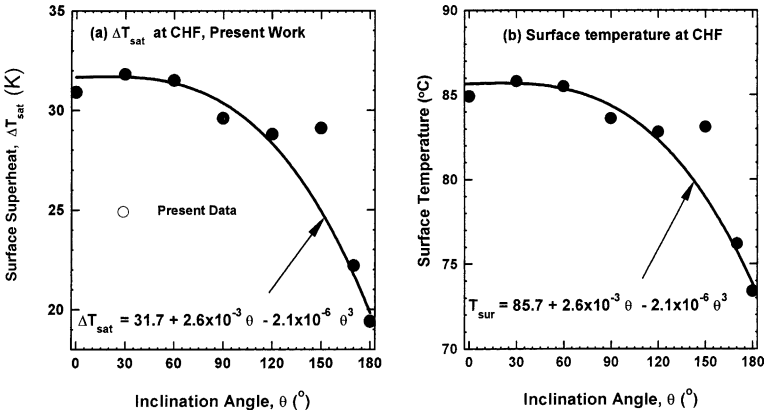

Fig. 13. The measured surface superheat and surface temperature at CHF for HFE-7100.

3.3. Photographs of boiling surface

Fig. 15a–f show some of the recorded still photographs of saturation nucleate boiling of HFE-7100 in the present experiments at $\theta = 0°$, 30°, 90°, 120°, 150°, and 180°, respectively, and at low, intermediate, and high nucleate boiling heat fluxes. These figures indicate that the increased accumulation of the vapor bubbles and void fraction near the surface with increased inclination cause both the nucleate boiling heat flux and CHF to decrease (Figs. 7c,8,9 and 10). At almost the same surface superheat, the nucleate boiling heat flux decreases with increasing inclination. For example, for $\theta = 0°$ and 90°, when $\Delta T_{sat} = 26.3$ and 26 K, respectively, the nucleate boiling heat flux is 22 and 26 W/cm^2, respectively (Figs. 12a and c). Similarly, for $\theta = 120°$ and 150°, when $\Delta T_{sat} = 25.1$ and 24.6 K, respectively, the nucleate boiling heat flux is 19.5 and 17.2 W/cm^2, respectively (Figs. 15c and f). In the downward-facing position, the heat removal from the copper surface by nucleate boiling is severely impaired due to the presence of large vapor masses near the surface (Fig. 15f). For almost the same surface superheat of ~18 K, the nucleate boiling heat flux for $\theta = 180°$ (Fig. 15f) is only 52% of that in the vertical position (90°) (Fig. 15c).

3.4. Departure bubble diameter

The departure bubble diameter in the present experiments is determined from the still photographs taken of nucleate boiling in the upward-facing position ($\theta = 0°$) at the lowest nucleate boiling heat flux, near that corresponding to incipient boiling (~0.5 W/cm^2). At this heat flux, the surface is not crowed with many growing bubbles. Several images of the boiling surface at this heat flux are recorded using high quality digital camera at a 3× magnification. The recorded images are then enhanced electronically and magnified by an additional 10× to 20×. It was then possible to identify a number of departing bubbles near the surface and measure their diameter. These processes are repeated for all other recorded images. The obtained values of the departing bubble diameters are consistent within an uncertainty of ±0.07 mm. The average departure bubble diameter measured from the photographs is 0.55 ± 0.07 mm. Measuring the departure bubble diameter in nucleate

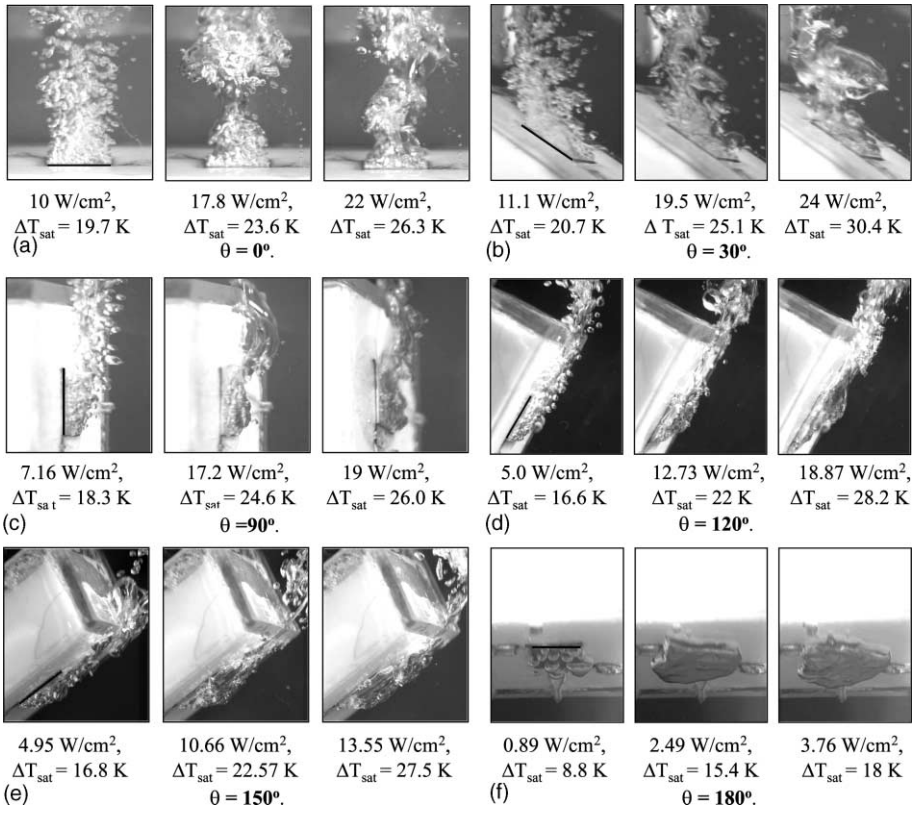

Fig. 15. Photographs of saturation nucleate pool boiling of HFE-7100 at different surface inclinations.

boiling has been the subject of numerous investigations for more than 60 years and recently for FC-72 [9], however, this is the first time a value is reported for HFE-7100. The departure bubble diameter, D_d, can be expressed in term of the Bond Number, *Bo*, as:

$$D_d = \left(\frac{Bo\sigma}{g(\rho_\ell - \rho_v)} \right)^{0.5}, \quad (7)$$

where *Bo* is given as [13]:

$$Bo = (0.04Ja)^2, \quad (8)$$

and

$$Ja = \left(\frac{\rho_\ell Cp_\ell \Delta T_{sat}}{\rho_v h_{fg}} \right). \quad (9)$$

In these equations, the liquid and vapor properties are evaluated at the saturation temperature in the experiments (at 0.085 MPa in Albuquerque, NM, see Table 1). At a surface superheat of 10.5 K the measured average nucleate boiling heat flux at incipient boiling of HFE-7100 at 0° is 0.5 W/cm^2 (Fig. 12a). For the same pressure and surface superheat, the calculated departure bubble diameters for saturated water and HFE-7100 using Eqs. (7) and (8) are 2.5 and 0.62 mm, respectively. The latter is about a fourth of that for water and only 13% larger than the measured value in the present experiments. The surface tension of HFE-7100 is about 18% of that of saturated water at 0.085 MPa, which explains the smaller departure bubble diameter for HFE-7100, compared to that for water.

Using the measured average departure bubble diameter for saturation boiling of HFE-7100 liquid (0.55 mm), the bubble departure frequency is calculated using the following relation [14]:

$$fD_d = 0.59 \left[\frac{\sigma g(\rho_\ell - \rho_v)}{\rho_\ell^2} \right]^{0.25}. \quad (10)$$

The calculated departure frequency is 100 s^{-1}, compared to only ~37 s^{-1} for saturated water at same surface superheat of 10.5 K and pressure of 0.085 MPa. This frequency corresponds to an average period of 10 ms between successive bubble departures from the surface in the present experiments.

4. Summary and conclusions

Experiments are performed, which investigated the effects of inclination angle on saturation pool boiling of HFE-7100 dielectric liquid from 1 cm^2 smooth, copper surface, simulating a high performance computer chip. The thermal analyses of the test section showed negligible heat losses from the side and the bottom of the test section and that the temperature of the copper surface is uniform and less than 0.2 K below that midway in the 1.63 mm thick copper block. Therefore, the average reading of the two thermocouples placed midway in the copper block is used as the surface temperature in the pool boiling curves.

The nucleate boiling heat flux and CHF decrease with increased θ from 0° to 180°. At 0° (upward-facing), CHF for HFE-7100 is 24.45 W/cm^2 and decreases slowly, almost linearly with increased θ to 90°, then rapidly to 4.30 W/cm^2 at 180°. For $\theta \leqslant 90°$ and $\Delta T_{sat} > 20$ K, nucleate boiling heat flux decreases with increased θ, due to the increase in vapor accumulation near the surface, but increases with increased θ at low surface superheats, due to the increase in mixing by rising bubbles in the boundary layer, whose residence time increases with increased inclination. These results are consistent with earlier data for dielectric and non-dielectric liquids. At higher inclinations ($\theta > 90°$) and $\Delta T_{sat} > 13$ K, the nucleate boiling heat flux decreases with increased θ, due to the increase in the accumulation of vapor bubbles near the surface. At lower surface superheats, however, the dependence of the nucleate boiling heat flux on inclination is inconclusive. The surface superheat at CHF also decreases with increasing θ. The developed correlations for saturation nucleate boiling heat flux and CHF as functions of θ agree with the present data for HFE-7100 to within ±10 and ±3%, respectively.

Despite the large difference between the CHF values for the FC-72 and HFE-7100 dielectric liquids, the normalized CHF values to that in the upward-facing position (0°) are almost identical and correlated as a function of θ with a maximum deviation of ±10% for $\theta < 170°$. For higher inclinations, this correlation is within ±20%–40% of the data for both HFE-7100 and FC-72, due to the sensitivity of the CHF measurement to the slightest adjustment in inclination near the downward facing position (180°). Results demonstrated that up to 24.5 W/cm^2 could be removed from a computer chip with smooth copper surface by saturation nucleate boiling of HFE-7100 at 0.085 MPa, which is ~57% higher than that reported earlier for the FC-72 at a slightly higher pressure (0.1 MPa).

The recorded still photographs of the nucleate boiling of HFE-7100 at different heat fluxes and $\theta = 0°$, 30°, 60°, 90, 120°, 150° and 180°, helped explain the measured dependency of the nucleate boiling heat flux and CHF on θ. The average departure bubble diameter of 0.55 ± 0.07 mm, determined from the photographs at $\theta = 0°$, is ~13% lower than calculated. The calculated bubble departure frequency based the measured average bubble diameter in the experiments is 100 s^{-1}.

Acknowledgement

The Institute for Space and Nuclear Power Studies at the University of New Mexico sponsored this research.

References

[1] D.A. Hall, Natural Convection Cooling of Vertical Rectangular Channels in Air Considering Radiation and Wall Conduction, Ph.D. Dissertation, The University of Texas at Austin, Austin, TX, 1997.

[2] G.P. Peterson, An Introduction to Heat pipes: Modeling, Testing, and Applications, Wiley, New York, 1994.

[3] R. Danielson, L. Tousignat, A. Bar-Cohen, Saturated pool boiling characteristics of commercially available perfluorinated inert liquids, Proc. ASME/JSME Thermal Eng. Joint Conf. 3 (1987) 419–430.

[4] Y. Chang, S. You, Heater orientation effects on pool boiling of micro-porous-enhanced surfaces in saturated FC-72, J. Heat Transfer 118 (11) (1996) 937–943.

[5] Y. Chang, S. You, Pool boiling heat transfer from inclined, micro-porous surfaces simulating microelectronic devices, ASME-EEP, vol. 19-2, Adv. Electronics Packaging 2 (1997) 2055–2063.

[6] K. Rainey, Pool Boiling Heat Transfer from Plain and Microporous Finned Surfaces in Saturated FC-72, Master's Thesis, The University of Texas at Arlington, Arlington, TX, 1999.

[7] A.C. McNeil, Pool Boiling Critical Heat Flux in a Highly Wetting Liquid, Master's Thesis, The University of Minnesota, Minneapolis, MN, 1992.

[8] M. Arik, A. Bar-Cohen, Ebullient Cooling of Integrated Circuits by Novec Fluids, Proc. Pacific Rim Int. Intersociety, Electronics Packaging Conference, Kauai, Hawaii, 18–13 July 2001.

[9] D. Rini, R. Chen, L. Chow, Bubble behavior and heat transfer mechanisms in FC-pool boiling, J. Expt. Heat Transfer 14 (1) (2001) 27–44.

[10] K. Nishikawa, Y. Fujita, S. Uchida, H. Ohta, Effect of heating surface orientation on nucleate boiling heat transfer, Proc. SME-JSME Thermal Eng. Joint Conf. 1 (1983) 129–136.

[11] M. El-Genk, Z. Guo, Transient boiling from inclined and downward-facing surfaces in a saturated pool, Int. J. Refrigeration 6 (1993) 414–422.

[12] S. Kutateladze, Boiling heat transfer, Int. J. Heat Mass Transfer 4 (1961) 31–45.

[13] R. Cole, Bubble frequencies and departure volumes at subatmospheric pressures, AIChE J. 13 (1967) 779–783.

[14] N. Zuber, Nucleate boiling—the region of isolated bubbles—similarly with natural convection, Int. J. Heat Mass Transfer 6 (1963) 53–65.